Scripta Materialia 230 (2023) 115399

Contents lists available at ScienceDirect

Scripta Materialia

journal homepage: www.journals.elsevier.com/scripta-materialia

Effect of molybdenum on recrystallization behavior of Fe30Mn5Al1C- x Mo lightweight austenitic steels

Kotla Sairam [a], M.P. Phaniraj [b], Korla Rajesh [a,*]

[a] Department of Materials Science and Metallurgical Engineering, Indian Institute of Technology Hyderabad, Kandi, Sangareddy, Telangana 502284, India
[b] Department of Metallurgical and Materials Engineering, Mahatma Gandhi Institute of Technology Gandipet, Hyderabad, Telangana 500075, India

ARTICLE INFO

Keywords:
Lightweight austenitic steels
Static recrystallization
Electron back scatter diffraction (EBSD)
Micro-indentation

ABSTRACT

Lightweight austenitic steels are among the materials of interest which can potentially reduce the CO_2 emissions and improve the fuel efficiency in automotive sector. Understanding the recrystallization behavior of these steels would open the door for a spectrum of structural applications that need a strength-ductility balance. In the present work, the recrystallization behavior of cold rolled Fe-30Mn-5Al-1C- (0–3 wt%) Mo austenitic steels after annealing at 600–1200 °C was investigated through EBSD, FESEM, TEM and hardness. The solubility of molybdenum in austenite and the equilibrium phases is determined through thermodynamic calculations. Alloying with more than 0.5 wt% Mo increased the recrystallization temperature by ~ 100 °C. M_2C type carbides precipitated in 2-Mo and 3-Mo alloys leading to grain refinement and delay in recrystallization. The hardness increased with increase in Mo content and decreased with increase in annealing temperature. At 1200 °C, due to grain growth all the alloys have similar grain size and hardness.

The development of steels with superior strength and ductility, to minimize the carbon-di-oxide emissions and improve the efficiency has been the goal of automotive sector. Lightweight steels based on Fe-Mn-Al-C system are finding interest due to their high specific strength and ductility. They offer reduced weight due to the lower atomic mass of aluminum and the dilation of iron lattice due to solute aluminum. The addition of aluminum and manganese alters the stacking fault energy of the steel and changes the deformation mechanism, which leads to better mechanical properties. These alloys are categorized based on the phases in their microstructure viz., ferritic, duplex (ferrite + austenite) and austenitic steels [1–5]. The austenitic class of steels drew attention owing to the precipitation hardening by intra-granular κ-carbide, $(Fe, Mn)_3AlC_x$ [6,7]. However, on long term aging the κ-carbide precipitates at the grain boundaries and deteriorates the mechanical properties [8,9]. Among the alloying additions, silicon accelerates the formation kinetics of κ-carbide [10,11], while molybdenum retards it [12]. It was also reported that alloying with up to 3 wt%Mo decreased the yield strength and beyond 4 wt% Mo increased it [13]. It was also shown that alloying with chromium along with molybdenum increased the resistance to pitting corrosion without loss in ductility [14].

The role of molybdenum in the precipitation of κ-carbide and control of mechanical properties is important. Static recrystallization is known to affect the grain size and thereby the mechanical properties. There is no literature on static recrystallization behavior of molybdenum alloyed lightweight austenitic steels. In the present work, we investigate the role of molybdenum on recrystallization behavior and hardness of Fe-30Mn-5Al-1C-*x*Mo lightweight austenitic steels.

Commercially pure iron, manganese, aluminum, molybdenum and graphite were vacuum induction melted to produce the alloys with four different Mo concentrations, Fe-30Mn-5Al-1C-*x*Mo (x = 0, 0.5,2 and 3 wt%). The chemical composition of the alloys obtained through ICP-MS presented in Table.1. The as cast alloys were homogenized at 1200 °C for 3hr, hot-forged and then hot-rolled to plates of 7 mm thickness. The hot-rolled plates were homogenized at 1100 °C for 2hr and cold rolled to 80% reduction in thickness. The cold rolled alloys were isochronally (1 h) annealed in the temperature range of 600–1200 °C under argon atmosphere to investigate the recrystallization behavior. EBSD (FESEM, JEOL, 7500 M) was used to characterize the microstructural evolution during annealing along with fraction recrystallized. Grain orientation spread (GOS) approach with GOS of 0–1.5° is used to distinguish recrystallized and deformed grains in the microstructure. The specimens for EBSD were prepared by grinding through a series of SiC papers and finish polishing by fine alumina (<0.5 μm) followed by electro polishing in 10% perchloric acid in methanol for 10 s at 20 V. The precipitates

* Corresponding author.
E-mail address: rajeshk@msme.iith.ac.in (K. Rajesh).

https://doi.org/10.1016/j.scriptamat.2023.115399
Received 1 November 2022; Received in revised form 5 January 2023; Accepted 28 February 2023
Available online 7 March 2023

Table. 1
Chemical composition of the alloys obtained through ICP-MS.

Alloy Designation	Chemical Composition (in wt%) Fe	Mn	Al	C	Mo
0-Mo	Bal	28.1 (±0.3)	4.5 (±0.1)	1.1(±0.1)	0
0.5-Mo	Bal	31.6 (±0.3)	5.1 (±0.1)	0.95 (±0.06)	0.51 (±0.01)
2-Mo	Bal	31.7 (±0.3)	4.9 (±0.1)	1.1(±0.1)	1.92 (±0.04)
3-Mo	Bal	31.2 (±0.3)	5.0 (±0.1)	1.1(±0.1)	2.94 (±0.05)

formed during annealing were identified using the Back Scattered Electron (BSE) imaging mode, TEM (JEM 2100F, JEOL) and SAED patterns. The TEM specimens were prepared by grinding to 80 μm thick, followed by twinjet polishing in the electrolyte 10% perchloric acid in methanol at 20 V and 200 mA at -30 deg.

Fig. 1a shows the GOS maps at different isochronal (1 h) annealing temperatures for all the alloys. Grains with grain orientation spread (GOS) less than 1.5°, considered as recrystallized grains were indicated with green color. Fig. 1b and c shows the fraction recrystallized (f_{rcx}) and grain size, respectively extracted from the GOS maps. It is clearly observed from Fig. 1a that the significant fraction of recrystallized grains were observed in case of 0-Mo compared to other alloys at 600 °C. The fraction recrystallized (%) increased with increase in the annealing temperature in all the alloys. At 700 °C, 0-Mo and 0.5-Mo alloys showed ~ 90% recrystallization, however 2-Mo and 3-Mo alloys showed ~50% and ~78% recrystallization respectively. The temperature at which ~90% recrystallization occurred is taken to be the recrystallization temperature in this study. The recrystallization temperature is 700 °C in 0-Mo and 0.5-Mo alloys, and is ~800 °C in 2-Mo and 3-Mo alloys. This indicates that molybdenum is retarding the recrystallization kinetics and increasing the recrystallization temperature by ~100 °C. At 800 °C and above, all the alloys showed greater than or equal to 90% recrystallization and grain growth. In general, in all the alloys grain size increased with increase in the annealing temperature and decreased with increase in molybdenum content. The difference in grain size between 0-Mo and 0.5-Mo as compared to 2-Mo and 3-Mo is initially significant up to 900 °C, whereas it is very minimal at 1200°C. However, in the 2-Mo and 3-Mo alloys, the grain size after annealing at different temperatures is similar. Fig. 2a shows the BSE micrograph of all the alloys after annealing at 700–1200 °C for 1 h. The alloys 0-Mo and 0.5-Mo shown a single-phase austenitic structure at all annealing temperatures. In 2-Mo and 3-Mo alloys, a secondary phase is present at the grain boundaries as well as in the matrix. This secondary phase, shown in inset figure (as well as in supplementary fig.S1) was distinctly observed on annealing from 700 °C up to 900 °C. At 1200 °C, secondary phase was not observed indicating its dissolution. Fig. 2b shows the TEM-SADP and EDS mapping of the 2-Mo alloy after annealing at 900 °C. The SADP of the matrix phase (marked as 1) confirmed the FCC structure and austenitic phase. The elemental mapping with the EDS detector showed that the

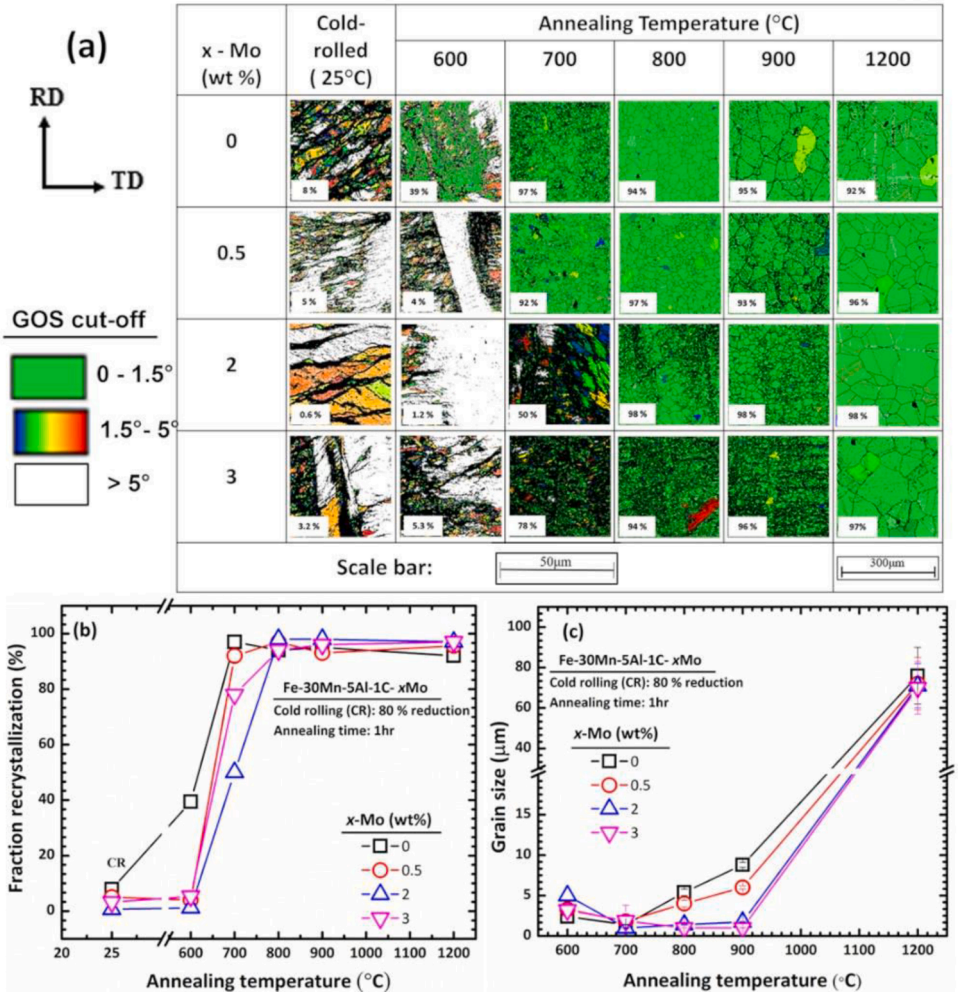

Fig. 1. Isochronally (1hr) annealed alloys showing: (a) Grain orientation spread maps with microstructural evolution, (b) recrystallization fraction (%) and **(c)** Grain size (in μm).

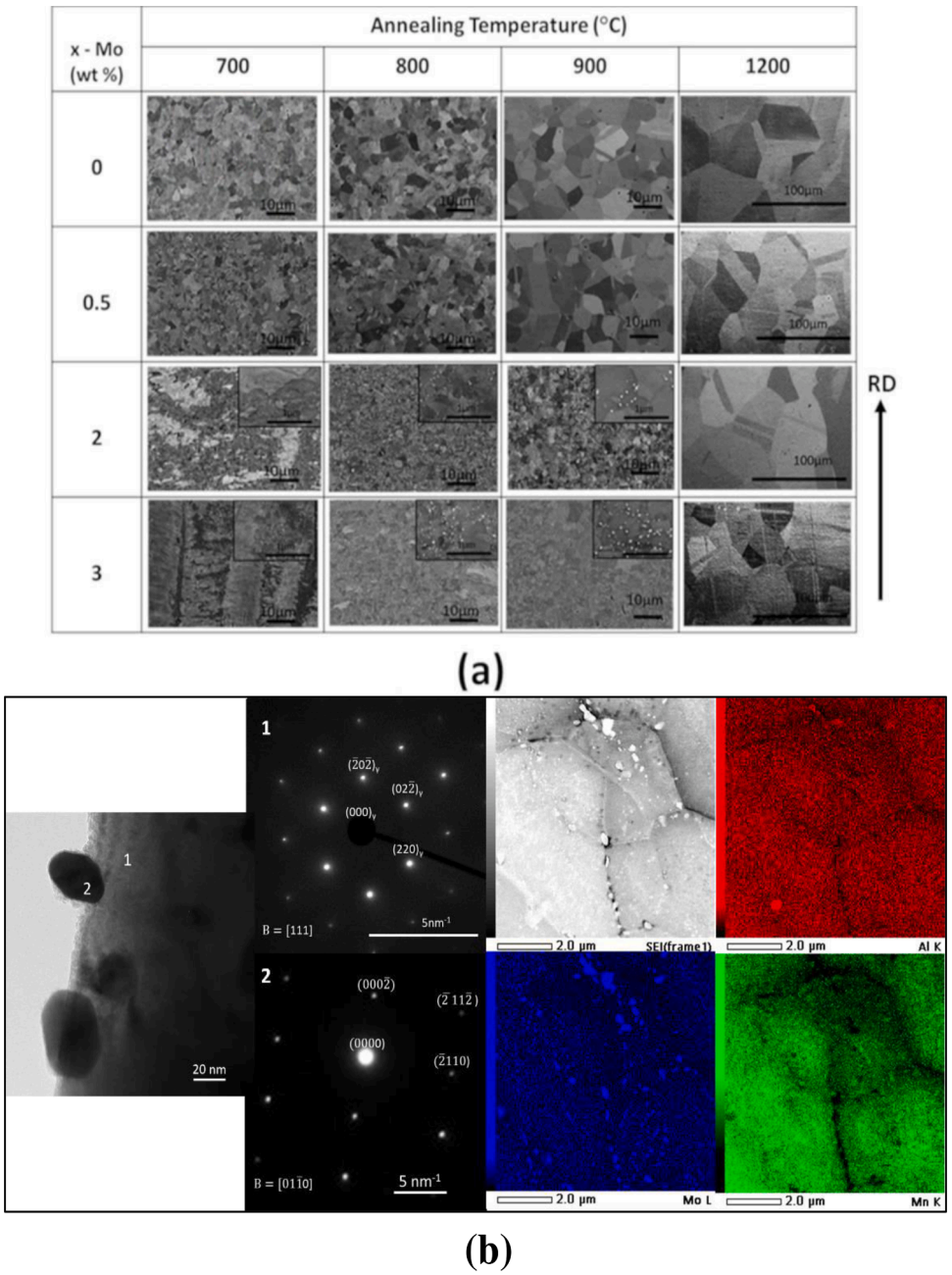

Fig. 2. (a) SEM micrographs of alloys with varying annealing temperatures showing the formation of Mo-rich precipitates, (b), TEM micrograph of 2Mo alloy annealed at 900 °C 1hr showing the austenite matrix and the Mo-rich carbide.

precipitates were rich in molybdenum and the SADP (marked as 2) revealed the precipitate to be hexagonal close-packed structure carbide. This is also confirmed by high-resolution TEM, EBSD phase map and Raman spectroscopic analysis (presented in supplementary Fig. S2, Fig. S3 and Fig.S4, respectively).

CALPHAD based Thermo-Calc software was used to predict thermodynamically equilibrium phases. The pseudo-binary phase diagram consisting of Fe-*x* Mo (for fixed Mn, Al and C), constructed using TCFE 9 data base, is shown in Fig. 3a. The composition of manganese, aluminum and carbon are taken as 30, 5 and 1 wt% respectively and iron is adjusted as balance for '*x*' wt% Mo. The equilibrium phases predicted (Fig.3a) in 2-Mo and 3-Mo alloys at temperature above 700 °C are austenite and M_2C with HCP structure. This confirms that the secondary phase present in the system as observed in Fig. 2b is molybdenum rich carbide (M_2C). The corresponding lattice constants calculated using [01–10] zone axis are $a = 4.67$ Å and $c = 7.4$Å These values are slightly higher compared to the lattice constants of Mo_2C [15] which may be due to the partitioning of Fe, Al and Mn to the Mo sublattice. Further, the formation of κ-carbide in the 0-Mo alloys is investigated by non-isothermal annealing at 550 °C for 5 min. Fig. 3b–d shows the bright field TEM micrograph and the high-resolution image with SADP in showing that there is no κ-carbide formed in the 0-Mo alloy.

From Fig 2a, it is observed that precipitation of M_2C and recrystallization are two events occurring during annealing of 2 and 3% Mo samples. Further, the precipitates are observed even at 700 °C where the alloys are in the partially recrystallized condition. The recrystallization of 2-Mo and 3-Mo alloys had resistance from secondary phase while not with the case of 0-Mo and 0.5-Mo alloys. The solubility limit of molybdenum in the austenite matrix could explain the differences in recrystallization among the alloys.

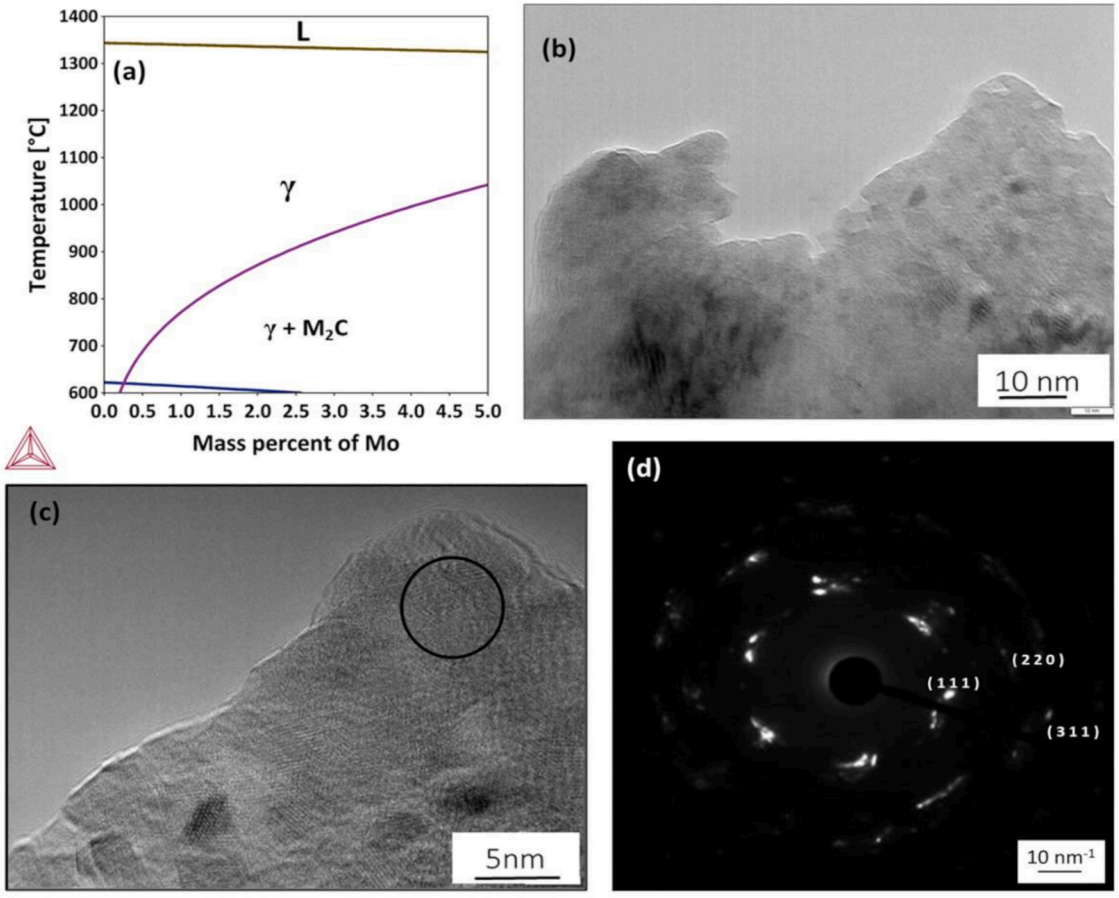

Fig. 3. (a) Pseudo binary phase diagram of Fe-Mo(Al-C-Mn fixed) showing the equilibrium between austenite (γ) and M_2C carbides at annealed temperatures,(b) Bright field TEM micrograph of 0-Mo alloy annealed non-isothermally at 550 °C for 5 min, and corresponding **(c)** High resolution TEM image, (d) SADP of selected regions showing no κ-carbide formation.

According to equilibrium thermodynamic calculations (Fig. 4a), the solubility of Mo in the alloy is upto 0.5 wt% at 700 °C. As a strong carbide former, the dissolved molybdenum present in the austenite matrix (up to 1.5 Mo) is having negative grain boundary-solute interaction energy which drags the grain boundary and makes the recrystallization and grain growth sluggish as compared to 0-Mo case[16]. This was further confirmed from the TEM-EDS Mo-concentration line profile for the 2Mo alloy annealed at 800 °C for 1 h, shown in Fig. 4b. It is observed that the molybdenum content was higher at grain boundary as compared to the grain interior. The average concentration of Mo obtained by EDS point spectrum at several locations both at the boundary and at the grain interior are 2.4 (±0.5) wt% and 1.4 (±0.35) wt% respectively. These observations clearly suggesting that molybdenum is segregating at the grain boundaries during annealing due to the

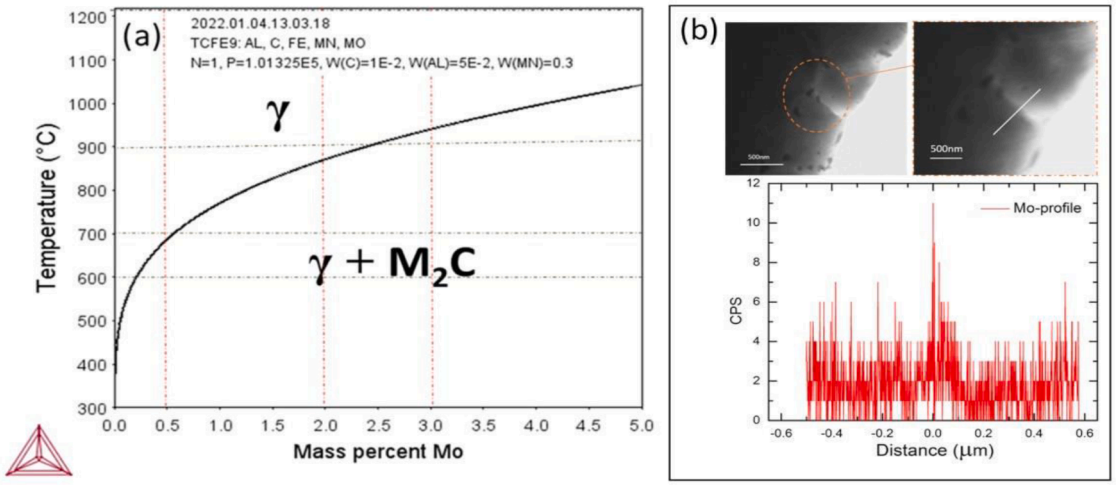

Fig. 4. (a) Solubility limit of molybdenum in austenite separated by austenite-austenite + M_2C phase boundary, (b) Molybdenum concentration profile across the grain boundary in 2-Mo alloy annealed at 800 for 1hr showing the segregation of molybdenum at grain boundary.

negative grain boundary-Mo solute interaction energy [16]. Therefore, the presence of Mo in the alloy can effect grain boundary migration due to solute drag, which can effect both recrystallization and grain growth kinetics. The solubility limit curve shows that with the increase in molybdenum beyond 0.5 Mo at 700 °C, the austenitic phase decomposes to austenite + M_2C precipitate. In the 2-Mo and 3-Mo alloys in addition to solute drag, the presence of M_2C precipitates also contributed to the grain refinement. These precipitates pin the grain boundaries and exert pressure against its migration. Thus, Zener pinning along with solute drag could be the two contributing factors for the grain refinement as well as shift in the recrystallization temperature in 2-Mo and 3-Mo alloys. At 1200 °C, there are no precipitates present in 2-Mo and 3-Mo alloys and consequently all the alloys have a similar grain size (~ 70–76 um).

The activation energy for grain growth was calculated using the grain sizes obtained after annealing (Fig. 1c) and the classical equation for isothermal grain growth. In Eq. (1) the growth exponent is assumed to be equal to 2.

$$d^n - d_0^n = k\ t = k_0.\exp\left(-\frac{Q}{RT}\right)t \tag{1}$$

where, t is the annealing time which is equal to 1 hr in the present work, d_0 is the initial grain size corresponding to annealing at 800 °C for 1 hr, d is the final grain size, n is grain growth exponent, k_0 is the pre-exponential constant, Q is the activation energy for grain growth and R is the gas constant. The activation energy for grain growth calculated as a function of Mo content is given in Table 2 and corresponding curves in supplementary Fig.4. The activation energy increases with the increase in the Mo content in both $n = 2$ and $n = 3$ and inhibits grain growth.

The strength of all the alloys is measured in terms of Vickers hardness. Fig. 5 shows the hardness of all the alloys after annealing at different temperatures. In general, the hardness increased with increase in Mo content and decreased with increase in annealing temperature in the alloys. The difference in the strength of the alloys can be explained in terms of the differences in their microstructure. In the 0-Mo and 0.5-Mo alloys, the microstructure is austenite, while in the 2-Mo and 3-Mo alloys the microstructure is austenite and M_2C precipitate. The hardness of 0-Mo alloy dropped readily with increase in annealing temperature while it increased slightly at 600 °C in other alloys before it continuously dropped. This observed difference could be due to segregation of molybdenum atoms during annealing. The difference in hardness among the alloys reduced with the increase in the annealing temperature. The significant difference in hardness (ΔH) between 0-Mo and 0.5-Mo is observed up to 700 °C, whereas between 2-Mo and 3-Mo, ΔH is observed up to 800 °C. This is because the alloys underwent complete recrystallization (>90%) by 700 °C and 800 °C, respectively.

The grain size and the hardness differences observed between 0-Mo and 0.5-Mo alloys convey that in 0.5-Mo, the strength contribution is from the grain refinement as well as the solid solution strengthening. However, in 2-Mo and 3-Mo alloys, along with the grain refinement and the solid solution strengthening, the precipitation strengthening also contributes to the strength. The hardness at 1200 °C is similar in all the alloys, which is consistent with the similar grain size in all the alloys (~70–76 μm).

Conclusion

The effect of molybdenum on recrystallization behavior of Fe-30Mn-5Al-1C-(0–3wt%) Mo alloys was investigated through the EBSD, FESEM, TEM and hardness. The microstructural evolution with annealing temperature and wt% of molybdenum was studied. The major conclusions drawn from the findings are:

Table. 2
The activation energy for the respective alloy found using the grain growth equation with grain size exponent equal to two.

Wt% Mo	Activation energy Q (kJ-mole^{-1})	
	$n = 2$	$n = 3$
0	231(±10)	326(±10)
0.5	250(± 70)	351(± 94)
2	385 (± 130)	540 (± 177)
3	450 (± 73)	760 (± 146)

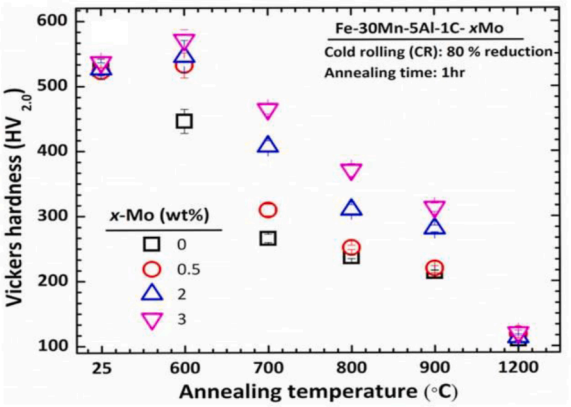

Fig. 5. Micro Vickers hardness of all alloys at different annealing temperatures.

(a) Alloying with more than 0.5 wt% molybdenum, increased the recrystallization temperature by ~ 100 °C, indicating retardation in the recrystallization kinetics.
(b) There are formation of Mo-enriched carbides in 2-Mo and 3-Mo alloys that affected the recrystallization kinetics.
(c) In the 0.5-Mo alloy, the solute-drag interface migration is responsible for delayed recrystallization. In the 2-Mo and 3-Mo alloys, pinning by the grain boundary precipitates (Zener drag) along with solute drag is responsible for the delayed recrystallization and grain growth.
(d) The increase in hardness upto 0.5 wt% Mo is a result of grain refinement along with solid solution strengthening whereas, in 2-Mo and 3-Mo alloys precipitation strengthening also contributed to hardness.

Declaration of Competing Interest

The authors declare that they have no known competing financial interests or personal relationships that could have appeared to influence the work reported in this paper.

Data availability

The raw/processed data required to reproduce these findings cannot be shared at this time as the data also forms part of an ongoing study.

Acknowledgments

The authors gratefully acknowledge, DMRL Hyderabad for melting and processing the alloys. The DST- CRG/2020/006207 for financial support and FE-SEM DST-FIST (SR/FST/ETI-421/2016) and JICA- Jeol F 200 with cold field emitter used for this work. The authors would like to thank Dr. Subhradeep Chatterjee, Dr. Sairama K Malladi, Dr. Shourya D Gupta, Dr. Saswata Bhattacharya at MSME department, IIT Hyderabad for their help in discussions.

Supplementary materials

Supplementary material associated with this article can be found, in the online version, at doi:10.1016/j.scriptamat.2023.115399.

References

[1] O. Grassel, L. Kruger, G. Frommeyer, L.W. Meyer, High strength Fe-Mn-(Al,Si) TRIP/TWIP steels development-properties-application, Int. J. Plast. 16 (2000) 1391–1409.

[2] R. Rana, C. Lahaye, R.K. Ray, Overview of lightweight ferrous materials: strategies and promises, JOM 66 (2014) 1734–1746.

[3] D. Raabe, H. Springer, I. Gutierrez-Urrutia, F. Roters, M. Bausch, J.B. Seol, M. Koyama, P.P. Choi, K. Tsuzaki, Alloy design, combinatorial synthesis, and microstructure-property relations for low-density Fe-MnAl-C austenitic steels, JOM 66 (2014) 1845–1856.

[4] H. Kim, D.W. Suh, N.J. Kim, Fe–Al–Mn–C lightweight structural alloys: a review on the microstructures and mechanical properties, Sci. Technol. Adv. Mater. (2013) 14.

[5] O.A. Zambrano, A general perspective of Fe–Mn–Al–C steels, J.Mater.Sci 53 (2018) 14003–14062.

[6] G.L. Kayak, Fe–Mn–Al precipitation-hardening austenitic alloys, Met. Sci. Heat Treat. 2 (95) (1969) 95–97.

[7] W.K. Choo, K.H. Han, Phase constitution and lattice parameter relationships in rapidly solidified $(Fe_{0.65}Mn_{0.35})_{0.83}Al_{0.17}$-x C and Fe_3Al-xC pseudo-binary alloys, Metall. Trans A 16 (1985) 5–10.

[8] C.N. Hwang, C.Y. Chao, T.F. Liu, Grain boundary precipitation in Fe-8.0Al-31.5Mn-1.05C, Alloys Scr. Metall. Mater. 28 (1993) 263–268.

[9] I. Gutierrez-Urrutia, D. Raabe, High strength and ductile low density austenitic FeMnAlC steels: simplex and alloys strengthened by nanoscale ordered carbides, Mater. Sci. Technol. 30 (2014) 1099–1104.

[10] L.N. Bartlett, D.C. Van Aken, J. Medvedeva, D. Isheim, N.I. Medvedeva, K. Song, An atom probe study of kappa carbide precipitation and the effect of silicon addition, Metall. Mater. Trans A 45 (2014) 2421–2435.

[11] C.W. Kim, M. Terner, J.H. Lee, H.U. Hong, J. Moon, S.J. Park, J.H. Jang, C.H. Lee, B.H. Lee, Y.J. Lee, Partitioning of C into κ-carbides by Si addition and its effect on the initial deformation mechanism of Fe-Mn-Al-C lightweight steels, J.Alloy. Compd. 775 (2019) 554–564.

[12] J. Moon, S.J. Park, J.H. Jang, T.H. Lee, C.H. Lee, H.U. Hong, D.W. Suh, S.H. Kim, H. N. Han, B.H. Lee, Atomistic investigations of κ -carbide precipitation in austenitic Fe-Mn-Al-C lightweight steels and the effect of Mo addition, Scr.Mater. 127 (2017) 97–101.

[13] J. Moon, S.J. Park, J.H. Jang, T.H. Lee, C.H. Lee, H.U. Hong, H.N. Han, J. Lee, B. H. Lee, C. Lee, Investigations of the microstructure evolution and tensile deformation behavior of austenitic Fe-Mn-Al-C lightweight steels and the effect of Mo addition, Acta Mater. 147 (2018) 226–235.

[14] J. Moon, H.Y. Ha, S.J. Park, T.H. Lee, J.H. Jang, C.H. Lee, H.N. Han, H.U. Hong, Effect of Mo and Cr additions on the microstructure, mechanical properties and pitting corrosion resistance of austenitic Fe-30Mn-10.5Al-1.1C lightweight steels, J. Alloy. Compd. 775 (2019) 1136–1146.

[15] S. Yamasaki, H.K.D.H. Bhadeshia, Modelling and characterisation of Mo_2C precipitation and cementite dissolution during tempering of Fe–C–Mo martensitic steel, Mater. Sci. Technol. 19 (2003) 723–731.

[16] H.K.D.H. Bhadeshia, Considerations of solute-drag in relation to transformation in steels, J. Mater. Sci. 18 (1983) 1473–1481.